Towards Opto-structural Correlation to Investigate Luminescence Thermometry in an Organometallic Eu(II) Complex

Roberto M. Diaz-Rodriguez,[†,§] Diogo A. Gálico,[†,§] Daniel Chartrand,[‡] Elizaveta A. Suturina,[¶] and Muralee Murugesu[†,*]

[†]Department of Chemistry and Biomolecular Sciences, University of Ottawa, Ottawa, Ontario K1N 6N5, Canada

[‡] Department of Chemistry, Université de Montréal, Montréal, Quebec H3T 1J4, Canada

[¶] Department of Chemistry, University of Bath, Claverton Down, Bath BA2 7AY, United Kingdom

ABSTRACT: Lanthanide-based luminescent materials have unique properties and are well-studied for many potential applications. In particular, the characteristic 5*d*→4*f* emission of divalent lanthanide ions such as Eu^{II} allows for tunability of the emissive properties via modulation of the coordination environment. We report the synthesis and photoluminescence investigation of pentamethylcyclopentadienyleuropium(II) tetrahydroborate bis(tetrahydrofuran) dimer (**1**), the first example of an organometallic, discrete molecular Eu^{II} band-shift luminescence thermometer. Complex **1** exhibits an absolute sensitivity of 8.2 cm^{-1} K^{-1} at 320 K, the highest thus far observed for a lanthanide-based band-shift thermometer. Opto-structural correlation via variable-temperature single-crystal X-ray diffraction and fluorescence spectroscopy allows rationalization of the remarkable thermometric luminescence of complex **1** and reveals the significant potential of molecular Eu^{II} compounds in luminescence thermometry.

Introduction

In recent years, materials based on molecular systems have shown remarkable optical/luminescent properties.[1–7] If such properties can be used to monitor changes in structure and/or temperature of the material, then applications employing these materials become viable. To that end, control over the interaction between light and matter is key to leading technological advancement in a wide range of fields. Molecular systems offer a remarkable advantage over traditional bulk materials when it comes to probing structural changes at the molecular level, and enable unparalleled flexibility to fine-tune the coordination environment around an emissive metal center. Structural parameters can be probed *via* single-crystal X-ray diffraction, while thermosensitive optical properties can provide subtle spectral changes with varying temperature. By careful association between the molecular structure and optical features, opto-structural correlation can be performed. Such analysis provides a unique insight into the connection between a material's structure and its optical properties. By taking advantage of such opto-structural correlation, an understanding of the factors that govern the change in physical properties is achievable, thus subsequent fine-tuneability of the optical properties becomes a reality.

When it comes to luminescent properties, trivalent lanthanide ions reign supreme, as they exhibit long-lived narrow emission lines which enable optical probing.[8] That being said, as the most stable divalent lanthanide ion, Eu^{II} is by far the most studied with respect to luminescence.[9] In contrast to most trivalent lanthanide ions, the presence of a low-lying 5*d* state gives rise to a strong *d*→*f* emission, allowed *via* selection rules. Luminescent molecular Eu^{II} compounds have been known for a long time, however studies involving them mostly focus on basic spectroscopic characterization.[10–18] Hence, applications of luminescent molecular Eu^{II} compounds[14,19–21] remain an underexplored area of study with tremendous potential. One such application is luminescence thermometry, wherein changes in the luminescence behaviour of a chemical probe as a function of temperature are used as a contactless temperature measurement technique.[1,2,6,22–29] Luminescence parameters of a probe that may vary with temperature include: emission peak energy; fluorescence lifetime and/or intensity; or the ratio of intensity between multiple emission bands, among others.[23,30–32]

In the family of divalent lanthanides, Sm^{II} and Eu^{II} are especially well-suited to this application, as their associated emissive *5d* state is very sensitive to the coordination environment.[33,34] Although luminescence thermometry has previously been achieved in Eu^{II}-containing inorganic materials,[35–45] it is surprising to note that no examples of discrete molecular Eu^{II} luminescence thermometers have been reported to date. This may be due to the highly air- and moisture-sensitive nature of most molecular divalent lanthanide compounds, making the synthesis, isolation and characterization of systems exhibiting the desired properties quite challenging. This is especially true of organometallic divalent lanthanide compounds, which are nevertheless highly desirable thanks to the unique stereoelectronic characteristics accessible using carbon-donor ligands. We therefore sought to explore avenues toward such compounds.

The small negative reduction potential of the Eu^{II}-Eu^{III} redox couple ($E°$ = -0.35 V)[46] allows the facile synthesis of $[Eu^{II}(BH_4)_2(THF)_2]$ from the reaction of $EuCl_3$ with $NaBH_4$, wherein Eu^{III} is reduced in situ.[7] This complex is unique among the simple lanthanide tetrahydroborates in that it displays intense blue luminescence in the solid state,[7,47] and yellow-green luminescence in THF solution. This observation implies that tetrahydroborate ligands are effective at sensitizing luminescence in Eu^{II}, making this compound a good starting point for the application-focused design of luminescent Eu^{II} compounds.

Tetrahydroborate ligands are coordinatively flexible and labile, often acting as pseudohalides in salt metathesis reactions, and are consequently well suited to the construction of more sophisticated complexes, including organometallic complexes.[48] Furthermore, Eu^{II} is isoelectronic to Gd^{III} ($4f^7$, with an $^8S_{7/2}$ ground state) and is accordingly highly paramagnetic. However, it is important to note that Gd^{III} is "optically silent", exhibiting no emissive transitions within the visible spectrum.[8] One can, therefore, envision applications employing Eu^{II} as a highly tunable luminescent analogue to its isoelectronic trivalent congener, the Gd^{III} ion. All considered, we surmised that $[Eu^{II}(BH_4)_2(THF)_2]$ could be a useful precursor for the preparation of exciting luminescent and optomagnetic molecular compounds.

Herein we report the synthesis, characterization, and photoluminescence of the divalent europium complex $[Cp^*Eu(\mu\text{-}BH_4)(THF)_2]_2$ (**1**). In the solid state, complex **1** acts as a highly sensitive band-shift luminescence thermometer operating over a broad temperature range (60-320 K), properties which are extremely sought-after for viability in such applications.[49] An opto-structural correlation study on this unique Eu^{II} luminescence thermometer highlights the versatility of molecular organometallic systems over traditional inorganic materials. The synthetic flexibility and stereoelectronic tunability afforded by organometallic constructs, combined with the remarkable luminescence properties of **1**, demonstrate the great potential of molecular Eu^{II} systems as luminescence thermometers, with incipient applications in the control of sensitive spintronic devices or organic electronics.

Results

Synthesis and structural characterization. The equimolar reaction of $[Eu^{II}(BH_4)_2(THF)_2]$ with potassium pentamethylcyclopentadienide (KCp*) in THF led to the formation of complex **1** as a microcrystalline yellow solid. Upon recrystallization from THF at -20 °C, transparent yellow, blocklike crystals suitable for X-ray crystallographic analysis were isolated. Complex **1** crystallizes in the monoclinic space group $P2_1/n$; the crystal structure is shown in Figures 1 and S1.

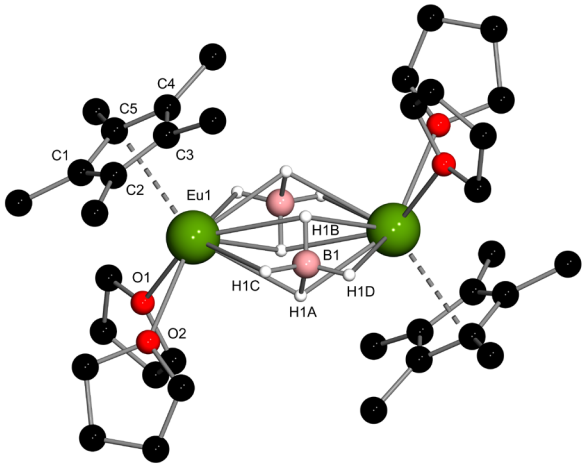

Figure 1. Molecular structure of **1**. Labels are given only to crystallographically unique atoms. Hydrogen atoms bonded to carbon have been omitted for clarity. A thermal ellipsoid diagram is shown in Figure S1. Selected bond lengths and angles are provided in Table S1.

The solid-state structure of **1** consists of a dimer where the Eu^{II} centers are bridged by two $(\mu_3\text{-}H)_2B(\mu_2\text{-}H)_2$ units,[50] with a monoanionic Cp* ligand and two molecules of THF completing the coordination environment of each Eu^{II} ion. It is noteworthy that **1** is only the second example of a bis(tetrahydroborate)-bridged homobimetallic Ln^{II} hemimetallocene, the first being the isostructural Sm^{II} complex $[Cp^*Sm(\mu\text{-}BH_4)(THF)_2]_2$ reported by Jaroschik *et. al.*, obtained *via* a similar synthetic route.[51] In the IR spectrum of **1** (Figure S2), a group of absorption peaks centered around 2260 cm^{-1} is observed. This spectral feature is reminiscent of that which was previously observed for $[(COT)Nd^{III}(BH_4)(THF)]_2$, which exhibits the same tetrahydroborate coordination mode as **1**.[52] Additionally, a pair of absorption peaks at 2243 and 2191 cm^{-1} are present, which comprise a doublet (splitting of 52 cm^{-1}) that is highly diagnostic of the $B\text{-}H_{bridging}$ stretch of a κ^3-tetrahydroborate.[53] Coordinated THF is also evidenced by the very strong absorption peaks at 881 and 1034 cm^{-1}. Attempts to observe **1** by ^1H NMR spectroscopy (Figure S3) revealed a resonance at +235 ppm attributable to the Cp* methyl substituents. The tetrahydroborate ligands could not be observed by ^1H or ^{11}B NMR spectroscopy, even when decoupled. This is unsurprising given the significant paramagnetic broadening from the two Eu^{II} centers, in conjunction with the quadrupolar broadening intrinsic to boron. The magnetic properties of **1** were measured (See Supporting Information), which confirmed the electronic structure of the complex as two isolated, isotropic $^8S_{7/2}$ ions, with weak ferromagnetic coupling appearing at very low temperatures. No decomposition was observed when crystalline **1** was stored for several months at -20 °C under inert atmosphere.

Photoluminescence. With the goal of understanding the spectroscopic features of **1** and rationalizing the potential of molecular organometallic Eu^{II} compounds as luminescence thermometers, the solid-state luminescence properties of single crystals of **1** were studied at varying temperatures. Excitation and emission spectra obtained at 10 K are shown in Figure 2.

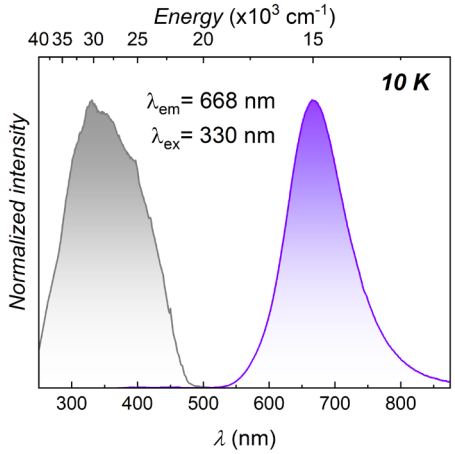

Figure 2. Excitation (gray) and emission (violet) spectra for **1** obtained at 10 K.

The excitation spectrum reveals bands from the Eu^{II} 5*d* state as well as ligand-based states over the UV and blue spectral region. Excitation at 330 nm results in a strong and broad $d \rightarrow f$ transition, as expected for divalent europium, centered at 669 nm (≈14959 cm^{-1}). Increasing the temperature does not

result in any spectral change until 60 K (Figure S9). However, above 60 K, a blue-shift of the band is observed, i.e., the band peak shifts to higher energies (Figures 3a and c). From 60 to 320 K, the emission maximum is shifted from 14959 to 16858 cm^{-1} (ΔE = 1899 cm^{-1}). Correspondingly, the output color of the emission is shifted from deep red to orange, as demonstrated on the *Commission Internationale de l'éclairage* (CIE) chromaticity diagram (Figure 3b). The observed shift of the band peak can be explored for band-shift based luminescence thermometry, as previously demonstrated for Sm^{II}, Eu^{III}, and Dy^{III} inorganic solids.[49] The energy shift can be fitted by a Boltzmann function (eq. 1) as implemented in OriginPro 2018 (see Figure 3c):

$$y = A_2 + \frac{(A_1 - A_2)}{1 + e^{[(x - x_0)/dx]}} \quad (1)$$

Absolute sensitivity S_a (Figure 3d) was calculated by taking the first derivative of the fitted function, and the maximum absolute sensitivity obtained was 8.2 $cm^{-1}\,K^{-1}$ at 320 K. This is the highest absolute sensitivity thus far observed for a lanthanide-based band-shift thermometer. For intensity-based luminescence thermometry methods, the intensity of a given luminescent probe varies with different equipment and experimental conditions. Contrarily, the position of the emission peak is an intrinsic property of a compound at a given temperature, independent of other factors. Therefore, absolute sensitivity is a reliable metric for comparing the performance of different band-shift thermometers. For completeness, we also report the relative sensitivity S_r (Figure S10) that shows lower relative performance. To further understand the thermometric performance of **1**, we evaluated the temperature resolution (ΔT). Values as low as 0.09 K are obtained (Figure S11), further confirming **1** as a highly competent band-shift luminescence thermometer.

The precursor compound $[Eu^{II}(BH_4)_2(THF)_2]$ itself demonstrates thermochromic luminescence (Figure S12), displaying a shift in the $d \rightarrow f$ emission band over the range 30 to 320 K from 19501 to 20679 cm^{-1} (ΔE = 1178 cm^{-1}); this represents a change in output colour from cyan to green. The maximum absolute sensitivity calculated for $[Eu^{II}(BH_4)_2(THF)_2]$ is 5.37 $cm^{-1}\,K^{-1}$ at 220 K. Table 1 compares the thermometric performance of our complex to other high-performing band-shift thermometers in the literature.

Table 1. Comparison of the highest-performing band-shift luminescence thermometers reported to date. Adapted from [49].

Thermometer	S_a ($cm^{-1}\,K^{-1}$)	Sensing Range (K)
Ag_2S quantum dots [54]	11	295-317
$[Cp^*Eu(\mu\text{-}BH_4)(THF)_2]_2$ [a]	8.2 @ 320 K	60-320
$\gamma\text{-}Al_2O_3:Sm^{II}$ [49]	8.0 @ 298 K[b]	298-648
$[Cp^*Eu(\mu\text{-}BD_4)(THF)_2]_2$ [a]	7.07 @260 K	30-320
$[Eu(BH_4)_2(THF)_2]$ [7,a]	5.37 @ 220 K	30-320
CdTe quantum dots [55]	5	300-353

[a] This work. [b] using the barycentre of the entire Sm^{II} emission band as the sensor.

While the thermometric performance of the precursor already matches that of some high-performing quantum-dot based sensors, complex **1** undergoes a 67% larger energy shift over its sensing range and exhibits a 53% improvement in sensitivity in comparison. Crucially, **1** emits in the red spectral range, thus has inherently higher temperature resolution than a blue-green emitter such as $[Eu^{II}(BH_4)_2(THF)_2]$. This is because the wavelength resolution of optical detectors is higher at longer wavelengths (see Supporting Information, Figure S11). As anticipated, **1** represents a unique example of an organometallic, discrete molecular Eu^{II}

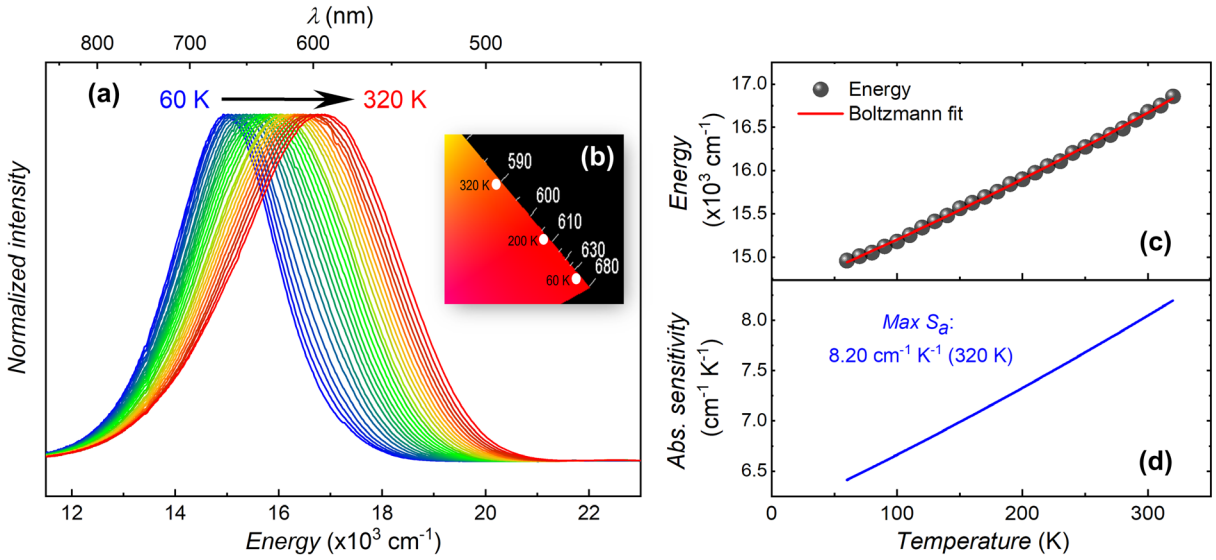

Figure 3. Temperature-dependent emission. **(a)** Temperature-dependent emission spectra (λ_{ex} = 330 nm) for **1** obtained in the solid state over the 60-320 K range with steps of 10 K. **(b)** Relevant section of the CIE diagram showing the luminescence colours of **1** at selected temperatures. **(c)** Temperature-dependence of the emission peak energy. The red line represents the Boltzmann function (eq. 1) used to fit the experimental data. Best-fitting parameters: r^2 = 0.999, A_1 = 8583, A_2 = 145840, and x_0 = 2920. **(d)** Absolute sensitivity obtained as the first derivative of the fitted function.

luminescence thermometer. The present result showcases the value of carbon-donor ligands in promoting high thermometric performance and suggests that molecular organometallic Eu^{II} compounds have tremendous potential as luminescence thermometers.

Variable-temperature structural analysis. To understand such luminescence thermometric behaviour and performance, it is critical to closely examine the molecular level. Especially, contrary to trivalent lanthanides, the *5d* orbitals involved in the $4f^6 5d^1$ excited-state configuration of Eu^{II} interact strongly with ligands, and thus the energy of the excited state and properties of the metal-centered luminescence are highly sensitive to ligand field effects.[9] Therefore, to elucidate the remarkable temperature-dependent emission of **1**, we carried out luminescence-structural correlation studies through variable-temperature single crystal X-ray crystallography within the range where thermometric behaviour was observed. The metrical parameters obtained from several crystal structures of **1** measured at 90, 175, 200, 203 and 270 K were carefully compared (Figure 4, Table S2 and Figure S14). We expected that variations in the Eu-ligand distances with temperature would be major contributors to the observed changes in luminescence with temperature, as is frequently the case for Ln^{II}-doped inorganic solids.[9,37,49,56] Surprisingly, however, the Eu-Cp*(cent) and Eu-O(THF) distances remain almost constant across the measured temperature range (within 0.004 and 0.006 Å, respectively). Meanwhile, the Eu-B distances increase by 0.03 Å with increasing temperature, concurrent with an equal increase in the B-B′ distances and an increase in the intramolecular Eu-Eu′ distance of 0.06 Å. The coordination geometry of a mononuclear fragment of **1** was analyzed using SHAPE 2.1 (Table S3 and Figure S15) and is best described as a distorted square pyramid around each Eu^{II} ion, with the ion above the basal plane of the pyramid. Notably, the complex increasingly distorts from the idealized square pyramidal geometry with increasing temperature, and furthermore, the Eu^{II} ions(s) migrate further from the basal plane (by 0.025 Å) with increasing temperature. As might be expected, the unit cell volume increases by 93.1 $Å^3$ (with a concomitant decrease in the crystal density of -0.06 g/cm^3), as does the closest intermolecular Eu-Eu distance (by 0.21 Å) with increasing temperature. From these data, a thermal expansion coefficient $\alpha_V = 2.54 \times 10^{-4}$ K^{-1} can be calculated for crystals of **1**,[37] consistent with the expectation for organic crystals.[57]

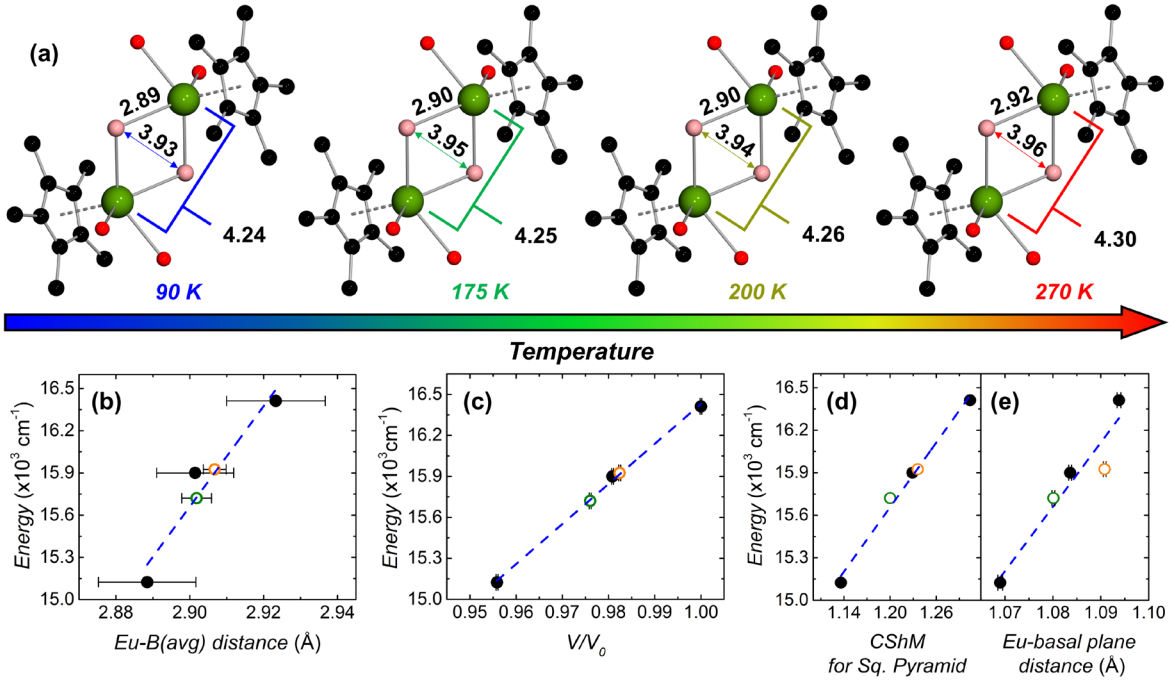

Figure 4. Variable-temperature structural analysis. **(a)** Temperature dependence of selected bond lengths from the crystal structure of **1**. The structure is truncated for clarity. Green = Eu, red = O, black = C, pink = B. Plots of emission peak energy as a function of the average Eu-B distance **(b)** and the relative compression of the lattice **(c)**. **(d)** Plot of emission peak energy as a function of the distortion of the coordination geometry around Eu. The distortion is represented by the continuous shape measure (CShM), which quantifies the deviation of the real coordination polyhedron from an idealized square pyramid. A value of zero represents exact agreement with the idealized geometry. **(e)** Plot of emission peak energy as a function of the distance between the Eu ion and the basal plane of the coordination pyramid, defined by the atoms B1, B1′, O1 and O2 (see Figure 1). The solid black points represent data collected from the same crystal at varying temperatures. The open green points represent data collected for a different crystal using the same diffractometer. The open orange points represent data collected on a different crystal using a different diffractometer. This demonstrates the consistency of the change in metrical parameters across the entire sample. Error bars are shown but overlap the points in some cases. The dashed blue lines are linear fits of the data to the equation y = mx+b. Best fitting parameters are as follows: **(b)** m = 35.7, b = -87.8, R^2 = 0.9108; **(c)** m = 29.3, b = -12.9, R^2=0.9975; **(d)** m = 7.6, b = 6.6, R^2 = 0.9875; **(e)** m = 45.4, b = -33.4, R^2 = 0.8810.

Over the selected temperature range (90-270 K), the emission peak energy increases by 1288 cm^{-1} (i.e., the emission peak is blue-shifted by 52 nm).

Structural effects on the optical properties. The thermochromism of **1** can be considered as a dynamic extension of the well-documented principles governing the emission peak energy in Eu^{II}-containing inorganic compounds, namely the geometry, ligand field splitting, metal-ligand covalency, and ligand polarizability of the coordination environment,[34,56,58–62] all of which are interrelated. The excited state configuration is strongly affected by the ligand field, as the overlap of the *5d* orbitals and the ligand orbitals is considerable.[9,62,63] These relatively strong interactions lead to significant variability of the *5d* manifold energy with the ligand field.[33,61] Metal-ligand covalency also increases as the polarizability of the ligand increases, leading to increasing red-shifts of the emitting state energy.[34,62] The deep red (i.e., low energy) emission of **1** at low temperatures is thus a result of the large ligand-field splitting imparted by the strongly donating Cp* ligand, in concert with the high polarizability of the tetrahydroborate ligands,[64] which favour lower-energy emitting states.[33] The pliability of borohydride lattices has been demonstrated to yield materials that are highly sensitive to pressure[60] and temperature,[37] consistent with the properties of our complex **1**. The structural changes observed in **1** point to an overall distancing of the ligands from the Eu^{II} ion with increasing temperature, e.g., the increasing volume of the crystalline lattice and lengthening of Eu-[BH_4] distances. It is well known that the lengthening of metal-ligand bonds decreases the strength of the ligand field exerted by the ligand(s), thereby decreasing the magnitude of the ligand field splitting (in this case, of the Eu^{II} $4f^{n-1}5d^1$ state).[9] This then drives the emitting level (lowest $f^{n-1}d^1$)[8] to higher energies and thus shorter emission wavelengths, as observed for **1** with increasing temperature (Figures 4b and 5, also see Figure S14e).

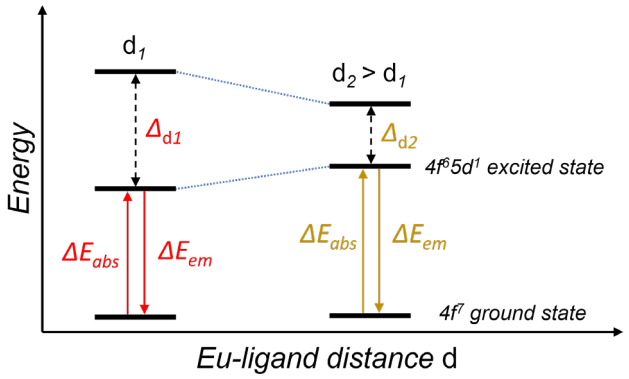

Figure 5. Schematic diagram of the general effect of Eu-ligand distance on ligand field splitting and emission peak energy in a Eu^{II} complex. The energy levels represent generalized "low-" and "high-" energy ligand-field states.

The magnitude of the change in transition energy as a function of Eu-[BH_4] bond length in **1** (*ca.* 37000 cm^{-1}/Å) is comparable to the analogous change as a function of Ce-Cl distance computed for Cs_2NaYCl_6:Ce^{III} (*ca.* 30000 cm^{-1} $Å^{-1}$), an archetypal lanthanide-doped inorganic solid with *5d→4f* emission. [59] The effects of the distortion of the square-pyramidal Eu^{II} coordination geometry (*vide supra*) must also be considered, as the change in position of the ion relative to the basal plane of the pyramid will influence the ligand-field splitting in the *5d* excited state.[65] Indeed, the emission peak energy of **1** correlates strongly to the magnitude of these distortions (Figure 4d and e). It has been demonstrated for octahedrally-coordinated *f*-element ions that the metal-ligand bond lengths shorten upon $f^n \rightarrow f^{n-1}d(t_{2g})^1$ excitation, regardless of the environment.[59,66–68] This contraction arises from a combination of the *5d* and ligand orbital interactions previously described and a stabilization of the *4f* hole generated in the excitation process *via* charge-transfer interactions with the ligands.[9,69] It is possible that the maximal excited-state bond contraction for **1** occurs at 60 K, below which no closer approach of the ligands to the central ion is possible, leading to the observed invariability of emission peak energy with temperature in the range 10-60 K.

To further investigate ligand effects on the thermochromic luminescence of **1**, an analogue bearing bridging tetradeuteroborate moieties (**1-BD_4**) was prepared, and its solid-state luminescence properties analyzed. **1-BD_4** exhibits slightly red-shifted luminescence at 10 K (674 nm ≅ 14839 cm^{-1}) *cf.* **1**, and a very similar blue-shift of the emission band peak with increasing temperature (Figure S17a, ΔE = 1858 cm^{-1}). However, the band shift of **1-BD_4** begins at 30 K, rather than 60 K as observed for **1**. While the emission peak energies of **1** and **1-BD_4** follow virtually the same trend with increasing temperature (Figure S17b), the peak energies of **1-BD_4** become increasingly lower *cf.* **1** at 150 K and above, though the largest difference in energy is only 158 cm^{-1} at 320 K. These slight differences cause the maximum absolute sensitivity of **1-BD_4** to be somewhat lower (7.07 cm^{-1} K^{-1}) than that of **1** and reach this maximum at a lower temperature (260 K) (Figure S17c). Due to the significantly higher mass of deuterium relative to protium, the vibrational energies of a B-D bond will be lower than an otherwise identical B-H bond. Indeed, these differences can be readily observed when comparing the IR spectra of **1** and **1-BD_4** (Figure S18), wherein the BX_4 vibrational band is shifted to lower energy by 630 cm^{-1}. The differences in emission peak energy between these complexes can thus be attributed primarily to the significantly different vibrational energies of the bridging BX_4 ligands, which manifests most obviously at higher temperatures. Table S4 compares the metrical parameters of **1** and **1-BD4** from crystal structures of each obtained at the same temperature (203 K). The average Eu-O(THF) distance and average of all Eu-ligand distances are longer in **1-BD_4** than **1**, but the average Eu-B distance is identical, and the intramolecular Eu-Eu distance is distinctly shorter. Most notably, **1-BD_4** has a larger unit cell volume (by 15 $Å^3$) than **1**, suggesting that the compressibility of crystals of **1-BD_4** may be higher than those of **1**. This, combined with the observation that the emission peak of **1-BD_4** begins shifting at lower temperature *cf.* **1**, supports the premise that the lower limit of the temperature sensing range is correlated with the compressibility of the lattice. This comparison further demonstrates the importance of the tetra(hydro/deutero)borate ligand(s) toward the thermochromic luminescence properties of these complexes. A comparison of the emission peak energies and sensitivities for each of [$Eu(BH_4)_2(THF)_2$], **1**, and **1-BD_4** are presented in Figure 6.

Time-dependent DFT calculations (Figure S19 and Tables S5 and S6) predict intense *4f→5d* absorption in the range 24-29000 cm^{-1}, consistent with the experimentally determined excitation profile (*vide supra*). However, these calculations also show a lower-energy charge transfer band involving the THF

ligands, which is not visible in the excitation profile. The energy of this predicted absorption band also changes substantially with increasing temperature (by ~1500 cm^{-1}). The *4f→5d* absorption bands calculated for the 90 and 270 K crystal structures of **1** have only a small energy shift, suggesting that the origin of the thermochromic luminescence might be more complex than a simple change in vertical transition energy; charge-transfer states intermediate to the *4f-5d* transition may play a role in the observed photoluminescence of complex **1**. The Hirshfeld surfaces of **1** at each temperature were analyzed, and only weak H-H and H-C intermolecular crystal packing interactions were observed (Figure S20), the strength and nature of which did not appear to correlate meaningfully with temperature. No intermolecular interactions whatsoever involving Eu, O or B were observed. It is thus unlikely that the thermochromic luminescence of **1** is due to intermolecular interactions. This opto-structural analysis suggests the thermochromism of **1** is dictated by the overall distortion of the Eu^{II} coordination environment with temperature, i.e., a simultaneous combination of all effects described above.

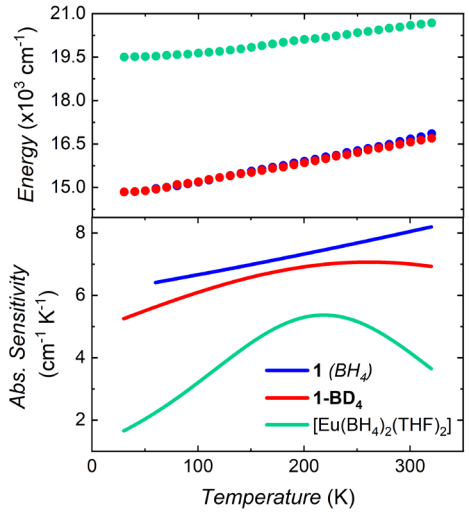

Figure 6. Comparison of the emission peak energy (top) and absolute sensitivity (bottom) of $[Eu(BH_4)_2(THF)_2]$, **1**, and **1-BD_4** as a function of temperature.

Conclusion

In summary, we report a notable example of an organometallic Eu^{II} molecular complex that acts as an efficient luminescence thermometer over a broad temperature range (60-320 K). The opto-structural correlation presented here represents a starting point for understanding how to modulate the thermometric performance of molecular Eu^{II} compounds. The high absolute sensitivity of 8.2 cm^{-1} K^{-1} obtained for complex **1,** the highest reported to date, reveals the potential of Eu^{II} compounds as viable molecular thermometers. The emission occurring in the red spectral region guarantees high temperature resolution. The emission peak energy of **1** is correlated with a change in Eu-ligand bond lengths, particularly of Eu-[BH_4] bonds, and other geometric distortions of the Eu^{II} coordination environment as a function of temperature, though charge-transfer interactions may also play a role in the observed emission. Further studies with different Eu^{II} complexes are anticipated to elucidate the exact origin of the temperature-sensitive luminescence and unlock the applicability of these compounds as luminescence thermometers through a deep and systematic study of how the structural features affect the band-shift behaviour.

Experimental

General. All manipulations were conducted under stringently oxygen- and moisture-free conditions under argon or nitrogen atmospheres using Schlenk line and glovebox techniques. All solvents were dried on columns of activated alumina using a J.C. Meyer Phoenix solvent system and degassed via repeated freeze-pump-thaw cycles, then stored over activated 4 Å molecular sieves. All reagents were purchased from STREM Chemicals, Sigma-Aldrich, or Fisher Scientific and used as received. Potassium pentamethylcyclopentadienide (KCp*)[70] and $[Eu(BH_4)_2(THF)_2]$[7] were prepared by reported procedures. $[Eu(BD_4)_2(THF)_2]$ was prepared according to the literature,[7] using protiated tetrahydrofuran rather than deuterated tetrahydrofuran. The $NaBD_4$ used was 98 atom % deuterium (Sigma).

Elemental analysis. Elemental analysis was performed by Midwest Microlab (Indianapolis, USA). Organolanthanide complexes, especially those of divalent ions, are well-known to suffer incomplete combustion and formation of carbides during microanalysis, yielding consistently and artificially low values.[20] Complexes bearing solvent ligands are further plagued by artificially low values due to loss of coordinated solvent during sample loading and/or combustion, thus microanalysis values should be considered within a wider tolerance than usually expected. Here, elemental analysis has been treated in a manner consistent with the literature regarding divalent organolanthanide compounds.

Infrared spectroscopy. Fourier transform infrared (FTIR) spectra were recorded in the $\tilde{\nu}$ = 4000-525 cm^{-1} range on a Nicolet Nexus 550 FTIR spectrometer equipped with an attenuated total reflectance (ATR) attachment. Samples comprised suspensions of crushed polycrystalline solid in a thin layer of Parabar 10312 oil; background spectra were corrected for the presence of the oil.

NMR spectroscopy. All NMR spectra were recorded using a Bruker AVANCE II 300 MHz spectrometer. Samples were prepared inside the glove box and sealed with a septum, Teflon tape and a layer of Parafilm to minimize incursion of air and moisture. ^1H chemical shifts are reported in ppm relative to tetramethylsilane using the THF-d_8 residual solvent signal at δ = 1.72 as an internal standard.

X-ray crystallography. X-ray crystallography of **1** and **1-BD_4** were performed using a Bruker AXS KAPPA single-crystal diffractometer equipped with an APEX II CCD detector, using graphite-monochromated Mo Kα radiation (λ = 0.71073 Å) from a sealed tube source. The crystals chosen were mounted on the tip of a 200 μm MicroLoop using Parabar 10312 oil and cooled to 203.15 K. Raw data collection and processing were performed with the Bruker APEX II software package.[71,72] A multi-scan absorption correction was applied (SADABS).[73] The crystal structures were solved via direct methods and refined using a full-matrix least-squares method on F^2 using the SHELXTL program suite[74–76] and the Olex2 user interface.[77] Non-hydrogen atoms were refined anisotropically. The

positions of all hydrogen atoms except for those bonded to boron were calculated based on the geometry of their respective atoms and are included at geometrically idealized positions [riding model]. Hydrogen atoms bonded to boron were located in the Fourier difference map and allowed to refine freely.

Variable-temperature X-ray structural analysis. Additional crystallographic analysis of **1** at varying temperatures (90, 175, 200, and 270 K) was performed using a Bruker D8 VENTURE METALJET single-crystal diffractometer equipped with a Photon III CMOS detector, using Ga Kα radiation (λ = 1.34139 Å) from a liquid Ga source (Bruker METALJET D2 PLUS with HELIOS MX optics). The crystals chosen were mounted on a loop fiber using Parabar 10312 oil and cooled to the indicated temperatures. Raw data collection and processing were performed as above, using the Bruker APEX 3 software package.[78–80] The H atoms of the BH_4 moieties were refined with an isotropic displacement parameter with a SADI restraint applied on all B-H distances. All other H atoms were generated geometrically and were included in the refinement in the riding model approximation; their temperature factors were set to a multiple of the equivalent isotropic temperature factors of the parent site (aromatic 1.2 times; methyl 1.5 times the factor). There was positional disorder of the Cp* moiety; the occupancy ratio was left to refine freely.

All diagrams were prepared using Diamond 4[81,82] or Mercury 2020.1[83] and POV-Ray.[84] The data has been deposited with the Cambridge Crystallographic Data Centre under deposition numbers 2107457-61 and 2126609. Analysis of the coordination geometry was performed using SHAPE 2.1,[85,86] using the THF oxygen atoms, centroid of the Cp* ligand, and the central boron atoms of the tetrahydroborate ligands as vertices. Hirshfeld surface analysis was performed using CrystalExplorer21.[87]

Photoluminescence spectroscopy. Photoluminescence data was obtained using a Horiba QuantaMaster 8075-21 spectrofluorometer. An ozone-free PowerArc 75 W xenon lamp was used as the radiation source. The excitation spectra were corrected in real time according to the lamp intensity and the optical system of the excitation monochromator using a silicon diode as a reference. The emission spectra were corrected according to the optical system of the emission monochromator and the photomultiplier response (Hamamatsu R13456 red-extended PMT). Samples were prepared inside the glove box and comprised a small amount of crystalline solid placed inside a screw-top quartz cuvette, which was then sealed with an additional layer of Teflon tape. Low-temperature measurements were performed with the samples mounted inside a CS202*E-DMX-1AL closed-cycle helium cryostat system (Advanced Research Systems), controlled via a LakeShore 335 temperature controller.

Magnetometry. Magnetic susceptibility measurements were performed using a Quantum Design MPMS-XL7 SQUID magnetometer operating in the temperature range 1.8-300 K. DC measurements were performed on crushed polycrystalline samples of **1** restrained in a matrix of vacuum grease (Corning) and wrapped in a polyethylene membrane. The magnetization data were collected at 100 K to check for ferromagnetic impurities, which were absent. Diamagnetic corrections were applied for the sample holder, and the inherent diamagnetism of the prepared sample was estimated with the use of Pascal's constants. $\chi_M T$ data was fitted using PHI 3.1.5.[88]

Synthesis of $[Cp^*Eu(BH_4)(THF)_2]_2$ (1). In a glove box under a positive pressure of nitrogen gas, $[Eu(BH_4)_2(THF)_2]$ (100 mg, 0.31 mmol) and KCp* (54 mg, 0.31 mmol) were dissolved in dry tetrahydrofuran (5 mL) with stirring. The solution immediately attained a yellow-orange colour, and orange luminescence was observed when the solution was excited with a 405 nm laser pointer. The mixture was stirred for 24 hr. at room temperature, during which a substantial quantity of precipitate formed. The mixture was filtered over a pad of Celite, and the pad rinsed with several 0.5 mL portions of tetrahydrofuran until the washings ran colourless. The filtrate was concentrated in vacuo until incipient crystallization, then tetrahydrofuran was added dropwise until all the solid just dissolved. The so-formed saturated solution was stored at -20 °C, resulting in the formation of yellow blocklike crystals. These were isolated by decantation of the supernatant and dried briefly under vacuum. This process was repeated with the supernatant to give **1** (71 mg, 51% yield over three crops). ^{1}H NMR (300 MHz, THF-d_8) δ: 235 ppm (s, Cp* methyl); $B(H)_4$ was not observed and coordinated THF could not be distinguished from residual THF. IR: $\tilde{\nu}$ = 2976 (w), 2939 (w), 2904 (w), 2883 (w), 2832 (vw), 2800 (w), 2715 (w), 2360 (m), 2318 (m), 2243 (m), 2191 (m), 1435 (br, m), 1340 (w), 1292 (w), 1246 (w), 1136 (m), 1105 (s), 1034 (vs), 881 (br, vs), 667 (br, m) cm^{-1}. Elemental analysis was consistent with the fully desolvated complex: Anal. calc'd. (%) for $C_{20}H_{38}B_2Eu_2$ (604.07) (**1** with loss of 4x coordinated THF): C, 39.77; H, 6.34. Found: C, 39.74; H, 6.63.

Synthesis of $[Cp^*Eu(BD_4)(THF)_2]_2$ (1-BD_4). Prepared following the same procedure as for **1** with $[Eu(BD_4)_2(THF)_2]$ (77 mg, 0.23 mmol) and KCp* (40 mg, 0.23 mmol) to give **1-BD_4** (50 mg, 48% yield over two crops). IR: $\tilde{\nu}$ = 2980 (s), 2943 (s), 2881 (s), 2839 (w), 2717 (w), 1768 (s), 1740 (s), 1680 (s), 1655 (s), 1576 (s), 1498 (w), 1435 (br, s), 1340 (w), 1294 (w), 1248 (w), 1176 (w), 1036 (vs), 881 (br, vs), 843 (s, sh), 800 (m, sh), 665 (br, s) cm^{-1}.

These compounds are highly air- and moisture-sensitive. Samples coated in Parabar oil appear to have increased stability and can be stored under ambient conditions for several days with only very slow decomposition. Decomposed samples present as off-white or pinkish powders rather than yellow crystalline solid.

ASSOCIATED CONTENT

Supporting Information. Infrared and ^{1}H NMR spectra, magnetic data, computational details, and additional photoluminescence and crystallographic information and analysis. This material is available free of charge via the Internet at http://pubs.acs.org.

AUTHOR INFORMATION

Corresponding Author

* Prof. Dr. M. Murugesu – *Department of Chemistry and Biomolecular Sciences, University of Ottawa, Ottawa, Ontario K1N 6N5, Canada;* Email: m.murugesu@uottawa.ca

Authors

Roberto M. Diaz-Rodriguez – *Department of Chemistry and Biomolecular Sciences, University of Ottawa, Ottawa, Ontario K1N 6N5, Canada.*

Diogo A. Gálico – *Department of Chemistry and Biomolecular Sciences, University of Ottawa, Ottawa, Ontario K1N 6N5, Canada.*

Daniel Chartrand – *Department of Chemistry, Université de Montréal, Montréal, Quebec H3T 1J4, Canada;*

Elizaveta A. Suturina – *Department of Chemistry, University of Bath, Claverton Down, Bath BA2 7AY, United Kingdom;*

Author Contributions

[§]R.M.D.-R. and D.A.G. contributed equally.

Notes

The authors declare no competing interests.

ACKNOWLEDGMENT

We thank the Canadian Foundation for Innovation (CFI), and the Natural Sciences and Engineering Research Council of Canada (NSERC) for financial support of this work. We thank Dr. Jeffrey Ovens and the uOttawa X-Ray Core Facility, as well as the X-Ray Diffraction Laboratory at the Université de Montréal, for access to crystallographic instrumentation and resources. We are thankful to thank Dr. A. A. Kitos (Murugesu Group) for useful discussions regarding crystallographic refinement.

REFERENCES

(1) Kitos, A. A.; Gálico, D. A.; Castañeda, R.; Ovens, J. S.; Murugesu, M.; Brusso, J. L. Stark Sublevel-Based Thermometry with Tb(III) and Dy(III) Complexes Cosensitized via the 2-Amidinopyridine Ligand. *Inorg. Chem.* **2020**, *59* (15), 11061–11070. https://doi.org/10.1021/acs.inorgchem.0c01534.

(2) Gálico, D. A.; Marin, R.; Brunet, G.; Errulat, D.; Hemmer, E.; Sigoli, F. A.; Moilanen, J. O.; Murugesu, M. Triplet-State Position and Crystal-Field Tuning in Opto-Magnetic Lanthanide Complexes: Two Sides of the Same Coin. *Chem. - A Eur. J.* **2019**, *25* (64), 14625–14637. https://doi.org/10.1002/chem.201902837.

(3) Parke, S. M.; Narreto, M. A. B.; Hupf, E.; McDonald, R.; Ferguson, M. J.; Hegmann, F. A.; Rivard, E. Understanding the Origin of Phosphorescence in Bismoles: A Synthetic and Computational Study. *Inorg. Chem.* **2018**, *57* (13), 7536–7549. https://doi.org/10.1021/acs.inorgchem.8b00149.

(4) Chan, K.-T.; Lam, T.-L.; Yu, D.; Du, L.; Phillips, D. L.; Kwong, C.-L.; Tong, G. S. M.; Cheng, G.; Che, C.-M. Strongly Luminescent Tungsten Emitters with Emission Quantum Yields of up to 84 %: TADF and High-Efficiency Molecular Tungsten OLEDs. *Angew. Chemie Int. Ed.* **2019**, *58* (42), 14896–14900. https://doi.org/10.1002/anie.201906698.

(5) Baudron, S. A. Luminescent Dipyrrin Based Metal Complexes. *Dalt. Trans.* **2013**, *42* (21), 7498–7509. https://doi.org/10.1039/c3dt50493j.

(6) Carlotto, A.; Babetto, L.; Carlotto, S.; Miozzi, M.; Seraglia, R.; Casarin, M.; Bottaro, G.; Rancan, M.; Armelao, L. Luminescent Thermometers: From a Library of Europium(III) β-Diketonates to a General Model for Predicting the Thermometric Behaviour of Europium-Based Coordination Systems. *ChemPhotoChem* **2020**, *4* (9), 674–684. https://doi.org/10.1002/cptc.202000116.

(7) Marks, S.; Heck, J. G.; Habicht, M. H.; Oña-Burgos, P.; Feldmann, C.; Roesky, P. W. [Ln(BH 4) 2(THF) 2](Ln = Eu, Yb)-A Highly Luminescent Material. Synthesis, Properties, Reactivity, and NMR Studies. *J. Am. Chem. Soc.* **2012**, *134* (41), 16983–16986. https://doi.org/10.1021/ja308077t.

(8) Bünzli, J. C. G. Lanthanide Luminescence: From a Mystery to Rationalization, Understanding, and Applications. *Handb. Phys. Chem. Rare Earths* **2016**, *50*, 141–176. https://doi.org/10.1016/bs.hpcre.2016.08.003.

(9) Suta, M.; Wickleder, C. Synthesis, Spectroscopic Properties and Applications of Divalent Lanthanides Apart from Eu 2+. *J. Lumin.* **2019**, *210* (October 2018), 210–238. https://doi.org/10.1016/j.jlumin.2019.02.031.

(10) Kim, J. M.; Jeong, Y. K.; Sohn, Y.; Kang, J. G. Synthesis and Photophysical Properties of an Eu(II)-Complex/PS Blend: Role of Ag Nanoparticles in Surface-Enhanced Luminescence. *Langmuir* **2012**, *28* (25), 9842–9848. https://doi.org/10.1021/la301547z.

(11) Jiang, J.; Higashiyama, N.; Machida, K. I.; Adachi, G. Y. The Luminescent Properties of Divalent Europium Complexes of Crown Ethers and Cryptands. *Coord. Chem. Rev.* **1998**, *170* (1), 1–29. https://doi.org/10.1016/S0010-8545(98)00070-8.

(12) Shinoda, S.; Nishioka, M.; Tsukube, H. In Situ Generation of Fluorescent Macrocyclic Europium(II) Complexes via Zinc Reduction. *J. Alloys Compd.* **2009**, *488* (2), 603–605. https://doi.org/10.1016/j.jallcom.2008.10.034.

(13) Pan, C. L.; Pan, Y. S.; Wang, J.; Song, J. F. A Heterometallic Sandwich Complex of Europium(Ii) for Luminescent Studies. *Dalt. Trans.* **2011**, *40* (24), 6361–6363. https://doi.org/10.1039/c1dt10635j.

(14) Zhan, G.; Wang, L.; Zhao, Z.; Fang, P.; Bian, Z.; Liu, Z. Highly Efficient and Air-Stable Lanthanide EuII Complex: New Emitter in Organic Light Emitting Diodes. *Angew. Chemie - Int. Ed.* **2020**, *59* (43), 19011–19015. https://doi.org/10.1002/anie.202008423.

(15) Kühling, M.; Wickleder, C.; Ferguson, M. J.; Hrib, C. G.; McDonald, R.; Suta, M.; Hilfert, L.; Takats, J.; Edelmann, F. T. Investigation of the "Bent Sandwich-like" Divalent Lanthanide Hydro-Tris(Pyrazolyl)Borates Ln(TpiPr2)2 (Ln = Sm, Eu, Tm, Yb). *New J. Chem.* **2015**, *39* (10), 7617–7625. https://doi.org/10.1039/c5nj00568j.

(16) Starynowicz, P. Complexes of Divalent Europium with Dotp and Dotpph. *New J. Chem.* **2021**, *45* (13), 5879–5889. https://doi.org/10.1039/d1nj00393c.

(17) Jenks, T. C.; Bailey, M. D.; Corbin, B. A.; Kuda-Wedagedara, A. N. W.; Martin, P. D.; Schlegel, H. B.; Rabuffetti, F. A.; Allen, M. J. Photophysical Characterization of a Highly Luminescent Divalent-Europium-Containing Azacryptate. *Chem. Commun.* **2018**, *54* (36), 4545–4548. https://doi.org/10.1039/c8cc01737a.

(18) Qi, H.; Zhao, Z.; Zhan, G.; Sun, B.; Yan, W.; Wang, C.; Wang, L.; Liu, Z.; Bian, Z.; Huang, C. Air Stable and Efficient Rare Earth Eu(Ii) Hydro-Tris(Pyrazolyl)Borate Complexes with Tunable Emission Colors. *Inorg. Chem. Front.* **2020**, *7* (23), 4593–4599. https://doi.org/10.1039/d0qi00762e.

(19) Qu, J.; Xia, Q.; Ji, W.; Jing, S.; Zhu, D.; Li, L.; Huang, L.; An, Z.; Xin, C.; Ni, Y.; Li, M.; Jia, J.; Song, Y.; Huang, W. A Ferrocene∩europium Assembly Showing Phototriggered Anticancer Activity and Fluorescent Modality Imaging. *Dalt. Trans.* **2018**, *47* (5), 1479–1487. https://doi.org/10.1039/c7dt04492e.

(20) Kelly, R. P.; Bell, T. D. M.; Cox, R. P.; Daniels, D. P.; Deacon, G. B.; Jaroschik, F.; Junk, P. C.; Le Goff, X. F.; Lemercier, G.; Martinez, A.; Wang, J.; Werner, D. Divalent Tetra- and Penta-Phenylcyclopentadienyl Europium and Samarium Sandwich and Half-Sandwich Complexes: Synthesis, Characterization, and Remarkable Luminescence Properties. *Organometallics* **2015**, *34* (23), 5624–5636. https://doi.org/10.1021/acs.organomet.5b00842.

(21) Shipley, C. P.; Capecchi, S.; Salata, O. V.; Etchells, M.; Dobson, P. J.; Christou, V. Orange Electroluminescence from a Divalent Europium Complex. *Adv. Mater.* **1999**, *11* (7), 533–536. https://doi.org/10.1002/(SICI)1521-4095(199905)11:7<533::AID-ADMA533>3.0.CO;2-U.

(22) Wang, J. X.; Yu, Y. S.; Niu, L. Y.; Zou, B.; Wang, K.; Yang, Q. Z. A Difluoroboron β-Diketonate Based Thermometer with Temperature-Dependent Emission Wavelength. *Chem. Commun.* **2020**, *56* (46), 6269–6272. https://doi.org/10.1039/d0cc01505a.

(23) Brites, C. D. S.; Balabhadra, S.; Carlos, L. D. Lanthanide-Based Thermometers: At the Cutting-Edge of Luminescence Thermometry. *Adv. Opt. Mater.* **2019**, *7* (5), 1801239. https://doi.org/10.1002/adom.201801239.

(24) Marin, R.; Brunet, G.; Murugesu, M. Shining New Light on Multifunctional Lanthanide Single-molecule Magnets. *Angew. Chemie - Int. Ed.* https://doi.org/10.1002/anie.201910299.

(25) Errulat, D.; Marin, R.; Gálico, D. A.; Harriman, K. L. M.; Pialat, A.; Gabidullin, B.; Iikawa, F.; Couto, O. D. D.; Moilanen, J. O.; Hemmer, E.; Sigoli, F. A.; Murugesu, M. A Luminescent Thermometer Exhibiting Slow Relaxation of the Magnetization: Toward Self-Monitored Building Blocks for Next-Generation Optomagnetic Devices. *ACS Cent. Sci.* **2019**, *5* (7), 1187–1198. https://doi.org/10.1021/acscentsci.9b00288.

(26) Bao, G.; Wong, K.-L.; Jin, D.; Tanner, P. A. A Stoichiometric Terbium-Europium Dyad Molecular Thermometer: Energy Transfer Properties. *Light Sci. Appl.* **2018**, *7* (1), 96. https://doi.org/10.1038/s41377-018-0097-7.

(27) Kitagawa, Y.; Kumagai, M.; Ferreira da Rosa, P. P.; Fushimi, K.; Hasegawa, Y. Long-Range LMCT Coupling in EuIII Coordination Polymers for an Effective Molecular Luminescent Thermometer**. *Chem. - A Eur. J.* **2021**, *27* (1), 264–269. https://doi.org/10.1002/chem.202002628.

(28) Outis, M.; Laia, C. A. T.; Oliveira, M. C.; Monteiro, B.; Pereira, C. C. L. A Europium(III) Complex with an Unusual Anion–Cation Interaction: A Luminescent Molecular Thermometer for Ratiometric Temperature Sensing. *Chempluschem* **2020**, *85* (3), 580–586. https://doi.org/10.1002/cplu.202000034.

(29) Wang, J.; Zakrzewski, J. J.; Zychowicz, M.; Vieru, V.; Chibotaru, L. F.; Nakabayashi, K.; Chorazy, S.; Ohkoshi, S. I. Holmium(Iii) Molecular Nanomagnets for Optical Thermometry Exploring the Luminescence Re-Absorption Effect. *Chem. Sci.* **2021**, *12* (2), 730–741. https://doi.org/10.1039/d0sc04871b.

(30) Quintanilla, M.; Liz-Marzán, L. M. Guiding Rules for Selecting a Nanothermometer. *Nano Today* **2018**, *19*, 126–145. https://doi.org/10.1016/j.nantod.2018.02.012.

(31) Zhao, Y.; Wang, X.; Zhang, Y.; Li, Y.; Yao, X. Optical Temperature Sensing of Up-Conversion Luminescent Materials: Fundamentals and Progress. *J. Alloys Compd.* **2020**, *817*, 152691. https://doi.org/10.1016/j.jallcom.2019.152691.

(32) Dramićanin, M. D. Trends in Luminescence Thermometry. *J. Appl. Phys.* **2020**, *128* (4), 040902. https://doi.org/10.1063/5.0014825.

(33) Lefevre, G.; Herfurth, A.; Kohlmann, H.; Sayede, A.; Wylezich, T.; Welinski, S.; Duarte Vaz, P.; Parker, S. F.; Blach, J. F.; Goldner, P.; Kunkel, N. Electron-Phonon Coupling in Luminescent Europium-Doped Hydride Perovskites Studied by Luminescence Spectroscopy, Inelastic Neutron Scattering, and First-Principles Calculations. *J. Phys. Chem. C* **2018**, *122* (19), 10501–10509. https://doi.org/10.1021/acs.jpcc.8b01011.

(34) Dorenbos, P. Energy of the First 4f 7 →4f 6 5d Transition of Eu 2+ in Inorganic Compounds. *J. Lumin.* **2003**, *104* (4), 239–260. https://doi.org/10.1016/S0022-2313(03)00078-4.

(35) Shi, R.; Ning, L.; Huang, Y.; Tao, Y.; Zheng, L.; Li, Z.; Liang, H. Li 4 SrCa(SiO 4) 2 :Eu 2+ : A Potential Temperature Sensor with Unique Optical Thermometric Properties. *ACS Appl. Mater. Interfaces* **2019**, *11* (10), 9691–9695. https://doi.org/10.1021/acsami.8b22754.

(36) Ruan, F.; Deng, D.; Wu, M.; Chen, B.; Lei, R.; Xu, S. Multichannel Luminescence of Eu2+/Eu3+ Co-Activated Ca9Mg1.5(PO4)7 Phosphors for Self-Referencing Optical Thermometry. *J. Lumin.* **2019**, *213* (May), 117–126. https://doi.org/10.1016/j.jlumin.2019.04.047.

(37) Wylezich, T.; Sontakke, A. D.; Castaing, V.; Suta, M.; Viana, B.; Meijerink, A.; Kunkel, N. One Ion, Many Facets: Efficient, Structurally and Thermally Sensitive Luminescence of Eu2+ in Binary and Ternary Strontium Borohydride Chlorides. *Chem. Mater.* **2019**. https://doi.org/10.1021/acs.chemmater.9b03048.

(38) Stefańska, D.; Stefanski, M.; Dereń, P. J. Unusual Emission Generated from Ca2Mg0.5AlSi1.5O7:Eu2+ and Its Potential for UV-LEDs and Non-Contact Optical Thermometry. *J. Alloys Compd.* **2021**, *863*, 1–7. https://doi.org/10.1016/j.jallcom.2021.158770.

(39) Ojo, A. O.; Fond, B.; Abram, C.; Van Wachem, B. G. M.; Heyes, A. L.; Beyrau, F. Thermographic Laser Doppler Velocimetry Using the Phase-Shifted Luminescence of BAM:Eu^2+ Phosphor Particles for Thermometry. *Opt. Express* **2017**, *25* (10), 11833. https://doi.org/10.1364/OE.25.011833.

(40) Chen, D.; Liu, S.; Wan, Z.; Ji, Z. EuF 3 /Ga 2 O 3 Dual-Phase Nanostructural Glass Ceramics with Eu 2+ /Cr 3+ Dual-Activator Luminescence for Self-Calibrated Optical Thermometry. *J. Phys. Chem. C* **2016**, *120* (38), 21858–21865. https://doi.org/10.1021/acs.jpcc.6b08271.

(41) Zhou, R.; Liu, C.; Lin, L.; Huang, Y.; Liang, H. Multi-Site Occupancies of Eu2+ in Ca6BaP4O17 and Their Potential Optical Thermometric Applications. *Chem. Eng. J.* **2019**, *369* (February), 376–385. https://doi.org/10.1016/j.cej.2019.03.073.

(42) Zhao, L.; Mao, J.; Jiang, B.; Wei, X.; Chen, Y.; Yin, M. Temperature-Dependent Persistent Luminescence of SrAl 2 O 4 :Eu 2+ , Dy 3+ , Tb 3+ : A Strategy of Optical Thermometry Avoiding Real-Time Excitation. *Opt. Lett.* **2018**, *43* (16), 3882. https://doi.org/10.1364/OL.43.003882.

(43) Zhou, X.; Geng, W.; Ding, J.; Zhao, Z.; Wang, Y. Ca 2 Na 2 La 6 (SiO 4) 4 (PO 4) 2 O: Eu 2+ /Eu 3+ : A Visual Dual-emitting Fluorescent Ratiometric Temperature Sensor. *J. Am. Ceram. Soc.* **2019**, *102* (9), 5443–5453. https://doi.org/10.1111/jace.16431.

(44) Yin, Z.; Fond, B.; Eckel, G.; Abram, C.; Meier, W.; Boxx, I.; Beyrau, F. Investigation of BAM:Eu(2+) Particles as a Tracer for Temperature Imaging in Flames. *Combust. Flame* **2017**, *184*, 249–251. https://doi.org/10.1016/j.combustflame.2017.06.005.

(45) Liu, W.; Liu, L.; Wang, Y.; Chen, L.; McLeod, J. A.; Yang, L.; Zhao, J.; Liu, Z.; Diwu, J.; Chai, Z.; Albrecht-Schmitt, T. E.; Liu, G.; Wang, S. Tuning Mixed-Valent Eu 2+ /Eu 3+ in Strontium Formate Frameworks for Multichannel Photoluminescence. *Chem. - A Eur. J.* **2016**, *22* (32), 11170–11175. https://doi.org/10.1002/chem.201602621.

(46) Morss, L. R. Thermochemical Properties of Yttrium, Lanthanum, and the Lanthanide Elements and Ions. *Chem. Rev.* **1976**, *76* (6), 827–841. https://doi.org/10.1021/cr60304a007.

(47) Sharma, M.; Didelot, E.; Spyratou, A.; Lawson Daku, L. M.; Černý, R.; Hagemann, H. Halide Free M(BH 4) 2 (M = Sr, Ba, and Eu) Synthesis, Structure, and Decomposition. *Inorg. Chem.* **2016**, *55* (14), 7090–7097. https://doi.org/10.1021/acs.inorgchem.6b00931.

(48) Visseaux, M.; Bonnet, F. Borohydride Complexes of Rare Earths, and Their Applications in Various Organic Transformations. *Coord. Chem. Rev.* **2011**, *255* (3–4), 374–420. https://doi.org/10.1016/j.ccr.2010.09.016.

(49) Ćirić, A.; Stojadinović, S.; Ristić, Z.; Zeković, I.; Kuzman, S.; Antić, Ž.; Dramićanin, M. D. Supersensitive Sm 2+ -Activated Al 2 O 3 Thermometric Coatings for High-Resolution Multiple Temperature Read-Outs from Luminescence. *Adv. Mater. Technol.* **2021**, *2001201*, 2001201. https://doi.org/10.1002/admt.202001201.

(50) Cendrowski-Guillaume, S. M.; Nierlich, M.; Lance, M.; Ephritikhine, M. First Chemical Transformations of Lanthanide Borohydride Compounds: Synthesis and Crystal Structures of [(η-C8H8)Nd(BH4)(THF)]2 and [(η-C8H8)Nd(THF)4][BPh4]. *Organometallics* **1998**, *17* (5), 786–

788. https://doi.org/10.1021/om9709446.
(51) Jaroschik, F.; Bonnet, F.; Le Goff, X.-F.; Ricard, L.; Nief, F.; Visseaux, M. Synthesis of Samarium(Ii) Borohydrides and Their Behaviour as Initiators in Styrene and ε-Caprolactone Polymerisation. *Dalt. Trans.* **2010**, *39* (29), 6761. https://doi.org/10.1039/c001795g.
(52) Cendrowski-Guillaume, S. M.; Le Gland, G.; Nierlich, M.; Ephritikhine, M. Lanthanide Borohydrides as Precursors to Organometallic Compounds. Mono(Cyclooctatetraenyl) Neodymium Complexes. *Organometallics* **2000**, *19* (26), 5654–5660. https://doi.org/10.1021/om000558f.
(53) Marks, T. J.; Kolb, J. R. Covalent Transition Metal, Lanthanide, and Actinide Tetrahydroborate Complexes. *Chem. Rev.* **1977**, *77* (2), 263–293. https://doi.org/10.1021/cr60306a004.
(54) Shen, Y.; Santos, H. D. A.; Ximendes, E. C.; Lifante, J.; Sanz-Portilla, A.; Monge, L.; Fernández, N.; Chaves-Coira, I.; Jacinto, C.; Brites, C. D. S.; Carlos, L. D.; Benayas, A.; Iglesias-de la Cruz, M. C.; Jaque, D. Ag2S Nanoheaters with Multiparameter Sensing for Reliable Thermal Feedback during In Vivo Tumor Therapy. *Adv. Funct. Mater.* **2020**, *30* (49). https://doi.org/10.1002/adfm.202002730.
(55) Liang, R.; Tian, R.; Shi, W.; Liu, Z.; Yan, D.; Wei, M.; Evans, D. G.; Duana, X. A Temperature Sensor Based on CdTe Quantum Dots-Layered Double Hydroxide Ultrathin Films via Layer-by-Layer Assembly. *Chem. Commun.* **2013**, *49* (10), 969–971. https://doi.org/10.1039/c2cc37553b.
(56) Srivastava, A. M.; Comanzo, H. A.; Camardello, S.; Chaney, S. B.; Aycibin, M.; Happek, U. Unusual Luminescence of Octahedrally Coordinated Divalent Europium Ion in Cs2M2+P2O7 (M2+=Ca, Sr). *J. Lumin.* **2009**, *129* (9), 919–925. https://doi.org/10.1016/j.jlumin.2009.03.018.
(57) Batsanov, A. S. Weak Interactions in Crystals: Old Concepts, New Developments. *Acta Crystallogr. Sect. E Crystallogr. Commun.* **2018**, *74*, 570–574. https://doi.org/10.1107/S2056989018005339.
(58) Poort, S. H. M.; Meyerink, A.; Blasse, G. Lifetime Measurements in Eu2+-Doped Host Lattices. *J. Phys. Chem. Solids* **1997**, *58* (9), 1451–1456. https://doi.org/10.1016/S0022-3697(97)00010-3.
(59) Ruiprez, F.; Seijo, L.; Barandiarán, Z. Prediction of Pressure-Induced Redshift of f 1 →d (t 2g) 1 Excitations in Cs 2NaYCl 6: Ce 3+ and Its Connection with Bond-Length Shortening. *J. Chem. Phys.* **2005**, *122* (23), 1–5. https://doi.org/10.1063/1.1935512.
(60) Schouwink, P.; Ley, M. B.; Tissot, A.; Hagemann, H.; Jensen, T. R.; Smrčok, ubomír; Černý, R. Structure and Properties of Complex Hydride Perovskite Materials. *Nat. Commun.* **2014**, *5* (May), 1–10. https://doi.org/10.1038/ncomms6706.
(61) Dorenbos, P. Relating the Energy of the [Xe]5d1 Configuration of Ce(3+) in Inorganic Compounds with Anion Polarizability and Cation Electronegativity. *Phys. Rev. B* **2002**, *65* (23), 235110. https://doi.org/10.1103/PhysRevB.65.235110.
(62) Andriessen, J.; Dorenbos, P.; Van Eijk, C. W. E. The Centroid Shift of the 5d Levels of Ce3+ with Respect to the 4f Levels in Ionic Crystals, a Theoretical Investigation. *Nucl. Instruments Methods Phys. Res. Sect. A Accel. Spectrometers, Detect. Assoc. Equip.* **2002**, *486* (1–2), 399–402. https://doi.org/10.1016/S0168-9002(02)00741-6.
(63) Aull, B. F.; Jenssen, H. P. Impact of Ion-Host Interactions on the 5d -to-4 f Spectra of Lanthanide Rare-Earth-Metal Ions. I. A Phenomenological Crystal-Field Model. *Phys. Rev. B* **1986**, *34* (10), 6640–6646. https://doi.org/10.1103/PhysRevB.34.6640.
(64) Albasiny, E. L.; Cooper, J. R. A. Amendments to the Calculated Polarizabilities of BH4-, CH4 and NH4+. *Proc. Phys. Soc.* **1963**, *82* (5), 801–802. https://doi.org/10.1088/0370-1328/82/5/116.
(65) Jurca, T.; Farghal, A.; Lin, P. H.; Korobkov, I.; Murugesu, M.; Richeson, D. S. Single-Molecule Magnet Behavior with a Single Metal Center Enhanced through Peripheral Ligand Modifications. *J. Am. Chem. Soc.* **2011**, *133* (40), 15814–15817. https://doi.org/10.1021/ja204562m.
(66) Valiente, R.; Rodríguez, F.; González, J.; Güdel, H. U.; Martín-Rodríguez, R.; Nataf, L.; Sanz-Ortiz, M. N.; Krämer, K. High Pressure Optical Spectroscopy of Ce3+-Doped Cs2NaLuCl6. *Chem. Phys. Lett.* **2009**, *481* (1–3), 149–151. https://doi.org/10.1016/j.cplett.2009.09.059.
(67) Grinberg, M. High Pressure Spectroscopy of Rare Earth Ions Doped Crystals-New Results. *Opt. Mater. (Amst).* **2006**, *28* (1–2), 26–34. https://doi.org/10.1016/j.optmat.2004.10.029.
(68) Mahlik, S.; Grinberg, M.; Shi, L.; Seo, H. J. Pressure Evolution of LiBaF3:Eu2+ Luminescence. *J. Phys. Condens. Matter* **2009**, *21* (23). https://doi.org/10.1088/0953-8984/21/23/235603.
(69) Joos, J. J.; Smet, P. F.; Seijo, L.; Barandiarán, Z. Insights into the Complexity of the Excited States of Eu-Doped Luminescent Materials. *Inorg. Chem. Front.* **2020**, *7* (4), 871–888. https://doi.org/10.1039/c9qi01455a.
(70) Monreal, M. J.; Thomson, R. K.; Cantat, T.; Travia, N. E.; Scott, B. L.; Kiplinger, J. L. UI4(1,4-Dioxane)2, [UCl4(1,4-Dioxane)] 2, and UI3(1,4-Dioxane)1.5: Stable and Versatile Starting Materials for Low- and High-Valent Uranium Chemistry. *Organometallics* **2011**, *30* (7), 2031–2038. https://doi.org/10.1021/om200093q.
(71) Inc., B. A. APEX II. Madison, Wisconsin, USA 2008.
(72) Inc., B. A. SAINT. Madison, Wisconsin, USA 2008.
(73) Inc., B. A. SADABS. Madison, Wisconsin, USA 2009.
(74) Sheldrick, G. M. A Short History of SHELX. *Acta Crystallogr. Sect. A Found. Crystallogr.* **2008**, *64* (1), 112–122. https://doi.org/10.1107/S0108767307043930.
(75) Sheldrick, G. M. SHELXT - Integrated Space-Group and Crystal-Structure Determination. *Acta Crystallogr. Sect. A Found. Crystallogr.* **2015**, *71* (1), 3–8. https://doi.org/10.1107/S2053273314026370.
(76) Sheldrick, G. M. Crystal Structure Refinement with SHELXL. *Acta Crystallogr. Sect. C Struct. Chem.* **2015**, *71* (Md), 3–8. https://doi.org/10.1107/S2053229614024218.
(77) Dolomanov, O. V.; Bourhis, L. J.; Gildea, R. J.; Howard, J. A. K.; Puschmann, H. OLEX2 : A Complete Structure Solution, Refinement and Analysis Program. *Journal of Applied Crystallography*. April 1, 2009, pp 339–341. https://doi.org/10.1107/S0021889808042726.
(78) Bruker AXS, I. APEX 3. Madison, Wisconsin, USA 2018.
(79) Bruker AXS, I. SAINT. Madison, Wisconsin, USA 2016.
(80) Bruker AXS, I. SADABS. Madison, Wisconsin, USA 2016.
(81) Putz, H.; Brandenburg, K. Diamond - Crystal and Molecular Structure Visualization. Bonn, Germany.
(82) Bergerhoff, G.; Berndt, M.; Brandenburg, K. Evaluation of Crystallographic Data with the Program DIAMOND. *J. Res. Natl. Inst. Stand. Technol.* **1996**, *101* (3), 221. https://doi.org/10.6028/jres.101.023.
(83) Macrae, C. F.; Bruno, I. J.; Chisholm, J. A.; Edgington, P. R.; McCabe, P.; Pidcock, E.; Rodriguez-Monge, L.; Taylor, R.; van de Streek, J.; Wood, P. A. Mercury CSD 2.0 – New Features for the Visualization and Investigation of Crystal Structures. *J. Appl. Crystallogr.* **2008**, *41* (2), 466–470. https://doi.org/10.1107/S0021889807067908.
(84) Buck, D. K.; Collins, A. A.; Enzmann, A. Persistence of Vision Ray Tracer (POV-Ray). 1991.
(85) Llunel, M.; Casanova, D.; Cirera, J.; Alemany, P.; Alvarez, S. SHAPE: Program for the Stereochemical Analysis of Molecular Fragments by Means of Continuous Shape Measures and Associated Tools. Barcelona, Spain 2013.
(86) Cirera, J.; Ruiz, E.; Alvarez, S. Continuous Shape Measures as a Stereochemical Tool in Organometallic Chemistry. *Organometallics* **2005**, *24* (7), 1556–1562. https://doi.org/10.1021/om049150z.
(87) Spackman, P. R.; Turner, M. J.; McKinnon, J. J.; Wolff, S. K.; Grimwood, D. J.; Jayatilaka, D.; Spackman, M. A. CrystalExplorer : A Program for Hirshfeld Surface Analysis, Visualization and Quantitative Analysis of Molecular Crystals. *J. Appl. Crystallogr.* **2021**, *54* (3), 1006–1011. https://doi.org/10.1107/S1600576721002910.

(88) Chilton, N. F.; Anderson, R. P.; Turner, L. D.; Soncini, A.; Murray, K. S. PHI: A Powerful New Program for the Analysis of Anisotropic Monomeric and Exchange-Coupled Polynuclear d- and f-Block Complexes. *J. Comput. Chem.* **2013**, *34* (13), 1164–1175. https://doi.org/10.1002/jcc.23234.

Authors are required to submit a graphic entry for the Table of Contents (TOC) that, in conjunction with the manuscript title, should give the reader a representative idea of one of the following: A key structure, reaction, equation, concept, or theorem, etc., that is discussed in the manuscript. Consult the journal's Instructions for Authors for TOC graphic specifications.

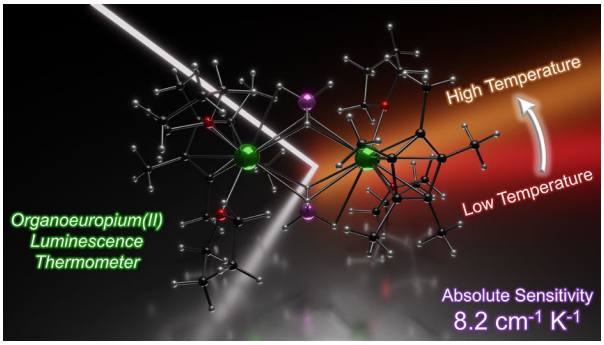

(For Table of Contents only)